Journal of Nuclear Materials 390–391 (2009) 255–258

Contents lists available at ScienceDirect

Journal of Nuclear Materials

journal homepage: www.elsevier.com/locate/jnucmat

Radiation process of carbon ions in JT-60U detached divertor plasmas

T. Nakano *, H. Kubo, N. Asakura, K. Shimizu, H. Kawashima, S. Higashijima

Japan Atomic Energy Agency, Mukoyama 801-1, Naka-shi, Ibaraki-ken 311-0193, Japan

A R T I C L E I N F O

PACS:
34.80.Lx
52.20.–j
52.25.Vy
52.55.Fa
52.55.Rk

A B S T R A C T

The spectral lines of C^{2+} and C^{3+} emitted around the X-point in the detached plasma with MARFE are measured with a VUV spectrometer and a two-dimensional visible spectrometer in order to compare the generation flux of C^{3+} (ionization of C^{2+} and recombination of C^{4+}) and the loss flux of C^{3+} (ionization and recombination of C^{3+}). It has been found that C^{3+} is produced by the volume recombination of C^{4+} and the ionization of C^{2+} comparably. In contrast, the volume recombination of C^{3+} is not detected, and the ionization flux of C^{3+} is less than 1% of the C^{3+} generation flux. Thus, the C^{3+} generation flux is higher by two orders of magnitude than the loss flux. This result suggests that another loss mechanism of C^{3+} such as transport loss from the X-point is significant.

1. Introduction

Heat and particle control in a fusion reactor depends on whether the plasma flowing into the divertor is cooled sufficiently and whether the cold plasma such as a detached plasma is maintained. Remote radiative cooling, which becomes effective in detached plasmas, is one of the most straightforward ways. In tokamak devices with carbon tiles such as JT-60U [1] and DIII-D [2], it has been found that C^{3+} is one of the most dominant radiators in divertor plasmas, which contributes more than 60% of the total radiation power although C^{2+} is the strongest radiator in JET [3].

However, the source of the radiators has not been known: from which region, the main plasma or the divertor target plates, they flow into the radiative zone. If the C^{3+} flux from the divertor region is higher than that from the main plasma, it is expected that auxiliary impurity seeded from the divertor, for instance, CD_4, ionizes into C^{3+} effectively and yields radiation efficiently, leading to high controllability of radiation loss. In contrast, if the C^{3+} flux from the main plasma is higher than that from the divertor region, the controllability of the radiation loss by auxiliary impurity seeding may be low because of difficulties in controlling the transport via the main plasma. Recently, it is reported that at the X-point in the detached plasma with MARFE, the volume recombination of C^{4+} is one of the processes to produce C^{3+} and that the electron temperature is too low to ionize C^{3+} to C^{4+} [4]. Hence it is expected that C^{4+} at the X-point is transported from the upstream via the main plasma, and is not originated from the lowly ionized carbon ions transported from the downstream of the divertor. However, it is not clear whether the volume recombination of C^{4+} is a dominant source of C^{3+} because this recombination flux is not compared to the ionization flux of C^{2+} to C^{3+}. In the present work, the excitation process of C^{2+} is investigated spectroscopically in order to determine the ionization flux of C^{2+} and the recombination flux of C^{3+}. From the comparison of these fluxes to the ionization flux of C^{3+} and the recombination flux of C^{4+} determined in Ref. [4], the C^{3+} generation and loss processes are discussed. Further the radiation power from C^{2+} is evaluated to compare it with that from C^{3+} determined in Ref. [4].

2. Experimental

Fig. 1 shows a schematic view of the poloidal cross-section of the JT-60U divertor. A W-shaped divertor is composed of baffles, divertor plates and a dome at the bottom of the vacuum vessel. Carbon fiber composite (CFC) materials are used for the divertor plates and the dome plates except for the inner dome wing plate. The toroidal-symmetric pumping slots are positioned between the divertor plates and the dome at the bottom of the divertor.

In Fig. 1 also shown are the viewing chords for the visible spectroscopic measurement. The divertor region is covered with a spatial resolution of ~1 cm by 60 vertical and 32 horizontal viewing chords. Emission from the divertor plasma is transmitted to a visible spectrometer through optical fibers. The visible range (350–800 nm) is covered with a grating with 300 grooves/mm. In the present experiment, the entrance slit width was set at 30 μm, leading to an instrumental width of 0.74 nm on the wavelength scale, and the frame rate of the CCD camera was set at 275 ms (an exposure time of 50 ms plus a digitization time of 225 ms). The detailed specification and setup of the spectrometer are found in Ref. [4]. With this spectrometer, the spectral lines of

---

* Corresponding author.
E-mail address: nakano.tomohide@jaea.go.jp (T. Nakano).

0022-3115/$ - see front matter © 2009 Elsevier B.V. All rights reserved.
doi:10.1016/j.jnucmat.2009.01.085

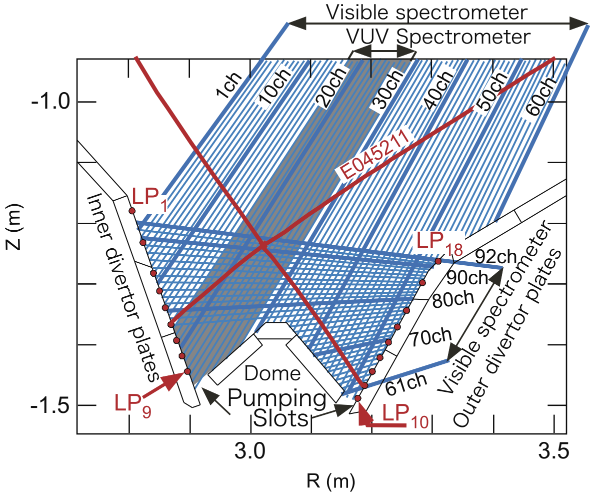

Fig. 1. The w-shaped divertor structure, the separatrix, the viewing chords (60 vertical and 32 horizontal) for the two-dimensional visible spectrometer, the viewing chord for the vacuum-ultra-violet spectrometer, and the positions of the Langmuir probes, which are indicated by LP with a subscript.

C III ($4f^3F-5g^3G:407.0$ nm), C III ($3s^3S-3p^3P:464.7$ nm), C III ($3p^1P-3d^1D:569.6$ nm) and C III ($5d^3D-6f^3F:748.7$ nm), were measured simultaneously with the 92 viewing chords.

In Fig. 1, the viewing chord for a VUV (Vacuum Ultra Violet) spectrometer [5] is shown, which corresponds to 17–29 ch of the viewing chords of the visible spectrometer. The spectral range of 20–120 nm is covered and the dispersion at a wavelength of 35 nm is 2.4 nm/mm. The absolute sensitivity of the spectrometer was calibrated by a branching ratio method. The determined sensitivity was nearly constant in the wavelength range of 30–70 nm, and this is consistent with the sensitivity relatively calibrated with a synchrotron radiation light source [6]. The detailed specification and setup of the spectrometer is found in Refs. [5,4], respectively. With this spectrometer, the spectral lines of C III ($2p^3P-3d^3D:45.96$ nm), C III ($2p^3P-3s^3S:53.83$ nm), C III ($2p^1P-3d^1D:57.43$ nm) and C III ($2s^1S-2p^1P:97.70$ nm) were measured simultaneously.

Fig. 1 shows the positions of Langmuir probes and the viewing chords of a bolometer, which are similar to the vertical viewing chords for the visible spectrometer although the spatial resolution is ~4 cm. Hereafter, the viewing chords of the bolometer are labeled by the viewing chord numbers corresponding to the vertical array for the visible spectrometer.

The present spectroscopic measurement was performed for an L-mode plasma at a plasma current of 1.0 MA and a toroidal magnetic field of 3.5 T with an X-point MARFE. In order to reduce statistical errors, the time-averaged intensities of the C III lines for 1.65 s (6 frames) during the MARFE phase are analyzed.

3. Analysis

The population densities of the excited levels of C^{2+} are analyzed with a collisional-radiative model. The collisional-radiative model also calculates a line-radiation energy rate per C III photon and ionization/recombination events per C III photon. By using these coefficients, the line-radiation power from C^{2+} and the recombination and the ionization flux are evaluated from the C III brightness.

3.1. Collisional-radiative model for C^{2+}

The temporal development of the population density of C^{2+}, $n_{C^{2+}(p)}$, is expressed as the differential equation,

$$\frac{d}{dt}n_{C^{2+}(p)} = -\left\{\sum_{q<p}A(p,q)+\sum_{q\neq p}C(p,q)n_e+S(p)n_e\right\}n_{C^{2+}(p)} + \sum_{q>p}A(q,p)n_{C^{2+}(q)} + \sum_{q\neq p}C(q,p)n_e n_{C^{2+}(q)} + \{\alpha(p)n_e+\beta(p)+\gamma(p)\}n_{C^{3+}}n_e + \sum_{n}q^{CX}(n,p)n_{D^0(n)}n_{C^{3+}}, \qquad (1)$$

which is coupled with similar equations for other levels. Here, p and q stand for a level that is determined by a principal quantum number n or combination of n and an azimuthal quantum number l. In Eq. (1), $q<p$ means that level q lies energetically lower than level p. The spontaneous transition probability from level p to level q is denoted by $A(p,q)$. The rate coefficients for electron impact excitation if $p<q$ (de-excitation if $p>q$) and ionization are denoted by $C(p,q)$ and $S(p)$, respectively. The rate coefficients for three-body, radiative and di-electronic recombination are denoted by $\alpha(p), \beta(p)$, and $\gamma(p)$, respectively. These rate coefficients are functions of electron temperature T_e. The rate coefficient for the charge exchange recombination from $D^0(n)$ to C^{3+} is denoted by $q^{CX}(n,p)$, which is a function of impact energy between $D^0(n)$ and C^{3+}. In Eq. (1), n_e, $n_{C^{3+}}$ and $n_{D^0(n)}$ denote electron density, C^{3+} density and $D^0(n)$ population density, respectively. The atomic data used in this model is similar to those for the collisional-radiative model for C^{4+} [4] except for the dielectric recombination rate coefficients, which are taken from the data calculated by Safronova et al. [7] for transitions to the $n\leqslant 6$ levels.

On the assumption that the quasi-steady-state solution is valid, the time derivative of Eq. (1) can be set at 0. Then the set of coupled differential equations reduces to the set of coupled linear equations. The steady-state solution for the population density of C^{2+} is obtained as

$$n_{C^{2+}(p)} = R_0(p)n_e n_{C^{2+}} + R_1(p)n_e n_{C^{3+}} + R_{CX}(p)n_{D^0}n_{C^{3+}}, \qquad (2)$$

where $n_{C^{2+}}$ denotes the ground-state density of C^{2+}. Here, $R_0(p)$ and $R_1(p)$ are population coefficients as functions of T_e and n_e, while $R_{CX}(p)$ is a population coefficient as functions of T_e, n_e, and the impact energy between D^0 and C^{3+}. The first term of Eq. (2) is referred to as the ionizing plasma component, $n^{\text{ioniz.}}_{C^{2+}(p)}$, the second term as the recombining plasma component, $n^{\text{recomb.}}_{C^{2+}(p)}$, and the third term as the charge exchange (CX) recombining plasma component, $n^{CX}_{C^{2+}(p)}$. The calculated population density of C^{2+} for the ionizing plasma component is shown in Fig. 2 as a function of the term energy of the upper level of the transition, or the energy from the ground state of C^{2+} (the ionization potential of C^{2+} is 47.9 eV). In comparison with the

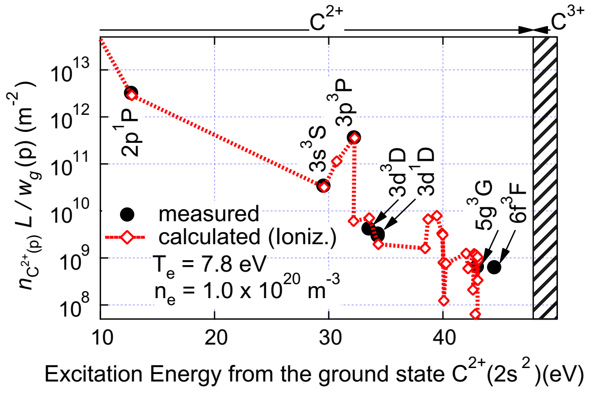

Fig. 2. Comparison of measured line-integral population density and fitted population density of the ionizing plasma component, divided by the statistical weight, as a function of excitation energy from the ground state of C^{2+}, or term energy of the excited level of C^{2+}. The ionization potential of C^{2+} is 47.9 eV.

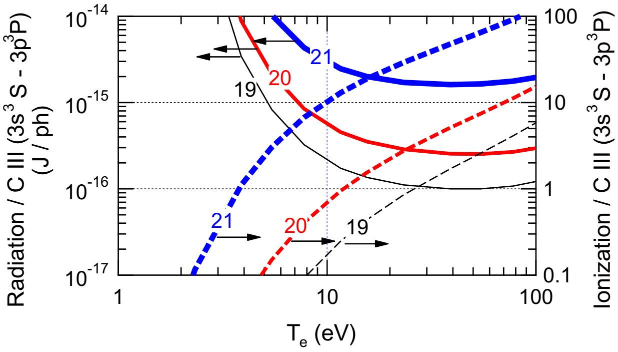

Fig. 3. (left) Line-radiation energy and (right) number of ionization events per a C III ($3s^3S-3p^3P$) photon for the ionizing plasma component, calculated by the collisional-radiative model. Numbers in the figure indicate decimal logarithm of n_e in m^{-3}.

measured population density, the population density is divided by the statistical weight, $w_g(p)$. Here, $w_g(p)=2p^2$ if p is the principal quantum number.

3.2. Line-radiation energy rate and ionization events per C III photon

The line-radiation power rate coefficients for the ionizing plasma component, $L^{\text{ioniz.}}_{C^{2+}}$, is expressed as follows:

$$L^{\text{ioniz.}}_{C^{2+}}=\sum_{p}\sum_{q<p}n^{\text{ioniz.}}_{C^{2+}(p)}A_{p,q}\Delta E(p,q)/(n_e n_{C^{2+}})\quad(\text{Wm}^3).\tag{3}$$

Here $n^{\text{ioniz.}}_{C^{2+}(p)}$ is population densities of the ionizing plasma component, which correspond to the first term of the right-hand-side of Eq. (2), and $\Delta E(p,q)$ is an absolute energy difference between the levels p and q.

The C^{2+} ionization flux $\Gamma_{C^{2+}\to C^{3+}}$ is expressed as follows:

$$\Gamma_{C^{2+}\to C^{3+}}=n_e n_{C^{2+}}S_{CR}\quad(\text{m}^{-3}\ \text{s}^{-1}).\tag{4}$$

Here, S_{CR} is a collisional-radiative ionization coefficient, which includes not only direct ionization to C^{3+} but also includes excitation to the excited revels of C^{2+} which finally ionizes to C^{3+}.

In order to evaluate the line-radiation power and the ionization flux of C^{2+} from the measured C III brightness, the line-radiation power rate coefficients and the number of ionization events, respectively, divided by the C III brightness are calculated with the collisional-radiative model. In Fig. 3, the line-radiation energy rate coefficient and the ionization flux per C III ($3s^3S-3p^3P$) for the ionizing plasma component are shown. The line-radiation energy rate coefficient increases significantly with decreasing electron temperature, in particular, in the electron temperature range below 10 eV. The number of C^{2+} ionization events per C III ($3s^3S-3p^3P$) indicates the opposite dependence on the electron temperature from the line-radiation energy rate per C III ($3s^3S-3p^3P$) photon.

4. Results

4.1. Population analysis

The line-integrated population density is inferred from the following equation, $n^{\text{meas.}}_{C^{2+}(p)}L=I(p,q)/A(p,q)(\text{m}^{-2})$. Here $I(p,q)$ (ph $\text{m}^{-2}\ \text{s}^{-1}$) is the measured C III brightness, and L(m) the length of the emission zone along a viewing chord. Further, the population density is divided by the statistical weight of the upper level of the transition, $w_g(p)$. Fig. 4 shows the line-integrated population density divided by the statistical weight. Similar spatial distribution is seen for the population densities of $n^{\text{meas.}}_{C^{2+}(p)}$ for $p=3p^3P, 3d^1D, 5g^3G$ and $6f^3F$: the population densities have a minimum around 23 ch (the X-point), are peaked on both sides of the X-point, and then decrease toward both the inner and the outer strike point. Because these two peaks are not resolved by the horizontal array, it is assumed that they are aligned along the same horizontal viewing chord 92 ch. As shown in Fig. 1, the volume that the VUV spectrometer observes includes the minimum and the peaks of C III emission. In Fig. 2, the population densities from the VUV C III lines are plotted together with those from the visible C III lines, which are volume-averaged for the same observation volume as the VUV spectrometer, which corresponds to the volume between 17 ch and 29 ch. To fit the measured population densities with those calculated by the collisional-radiative model, a regression analysis was performed with the electron temperature, the electron density, the neutral deuterium density and the ratio of C^{3+} to C^{2+} density as the free parameters, on the assumption that temperatures of a neutral deuterium and a C^{3+} ion were equal to the electron temperature. As shown in the figure, the result of the regression analysis indicates that the ionizing plasma component dominates the population density, meaning that the recombining plasma component is not detected. The determined electron temperature and density are 7.8 eV and $1.0\times10^{20}\ \text{m}^{-3}$, respectively. Note that the charge exchange recombining plasma component is absent because the residual between the regression curve and the measured population densities becomes large with increasing neutral deuterium density over zero. The mean-free-path of a neutral deuterium, calculated from an ionization rate coefficient ($7.3\times10^{-15}\ \text{m}^3\ \text{s}^{-1}$) at an electron temperature of 7.8 eV and density of $1.0\times10^{20}\ \text{m}^{-3}$, taken from Ref. [8], is 3.5 cm on the assumption that the neutral deuterium temperature is equal to the electron temperature. Given that the spatial spread of the strong C III emission zone is ~20 cm as shown in Fig. 4, where the viewing chord interval is ~1 cm, it is considered that the neutral deuterium penetration into this zone is limited. This estimation supports the collisional-radiative model analysis, which resulted in absence of the charge exchange recombining plasma component.

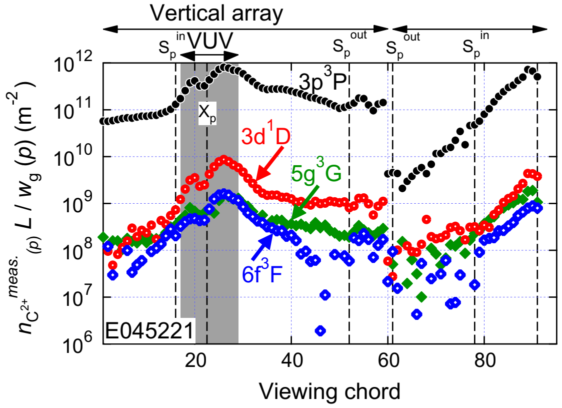

Fig. 4. Spatial profile of measured line-integrated population density $n^{\text{meas.}}_{C^{2+}(p)}L$, divided by the statistical weight of the level $w_g(p)$. The inner and the outer strike point are denoted by S^{in}_p and S^{out}_p, respectively, and the X-point by X_p.

Similar analysis for C IV [4] indicated that the recombining plasma component dominated the population density with levels ⩾5 of C IV, which term energies are higher than 55 eV. This supports that the population densities of all the levels of C III is dominated by the ionizing plasma component because the ionization potential of C III (47.9 eV) is lower than the term energy of the $n=5$ level of C IV (~56 eV).

4.2. Radiation power from the ionizing plasma component and ionization flux

The radiation power from the ionizing plasma component is evaluated from the absolute intensity of C III ($3s^3S-3p^3P$) with

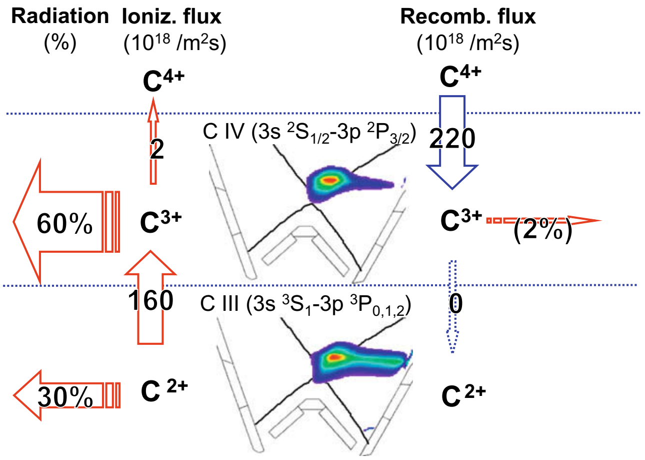

Fig. 5. From the left, the radiation power from the ionizing plasma component, the ionization flux, the spatial distribution of the emissivity, the recombination flux, and the radiation power from the recombining plasma component of C^{3+} (upper) and C^{2+} (lower).

the coefficient shown in Fig. 3. Given that the absolute intensity of C III ($3s^3S - 3p^3P$) averaged between the viewing chords 17 ch and 29 ch, which correspond to the viewing chord of the VUV spectrometer, is 4.0×10^{20} ph m^{-2} s^{-1} and that the ‘radiation/C III ($3s^3S - 3p^3P$)’ coefficient at an electron temperature of 7.8 eV and an electron density of 1.0×10^{20} m^{-3} is 1×10^{-15} J ph^{-1}, then the radiation power of the ionizing plasma component is estimated to be 0.4 MW m^{-2}, which corresponds to 30% of the total radiation power measured by the bolometer, 1.4 MW m^{-2}.

As already described in Fig. 3, the ‘radiation/C III ($3s^3S - 3p^3P$)’ coefficient is very sensitive to electron temperature particularly below 10 eV. Thus, the accuracy of the evaluated radiation power depends significantly on the accuracy of the determined electron temperature, indicating that the C III ($3s^3S - 3p^3P$) line is not a good measure for the radiation power at a low electron temperature of 7.8 eV. This is because the excitation rate to the 3p level from the ground state of C^{2+} is much lower than that to lower excited levels such as the 2p level, the lines from which are still main contributors to the radiation. Therefore, the line such as C III ($2s^1S - 2p^1P : 97.70$ nm) is a better measure for the radiation power, although the error of the absolute intensity may be significant because of difficulties of sensitivity calibration in the VUV range.

The ionization flux of C^{2+} is evaluated in a similar way to the radiation power evaluation. As shown in Fig. 3, the ‘ionization/C III ($3s^3S - 3p^3P$)’ coefficient is 0.4 at an electron temperature of 7.8 eV and an electron density of 1.0×10^{20} m^{-3} and the absolute intensity of the C III line is 4.0×10^{20} ph m^{-2} s^{-1}, leading to the C^{2+} ionization flux of 1.6×10^{20} m^{-2} s^{-1}.

5. Discussion and summary

From the above results and the results of Ref. [4], the radiation power and the balance of the ionization and the recombination fluxes were investigated. The results are summarized in Fig. 5. The line-radiation power from the ionizing plasma component of C^{2+} and C^{3+} were evaluated to be, respectively 30% and 60% of the total radiation power while the line-radiation power from the recombining plasma component of C^{3+} was only a few percent. The C^{3+} production flux, i.e., the recombination flux of C^{4+} into C^{3+} and the ionization flux of C^{2+} into C^{3+} were, respectively, 220 and 160×10^{18} m^{-2} s^{-1}. In contrast, the C^{3+} loss flux, i.e., the recombination flux of C^{3+} into C^{2+} was not detected and the ionization flux of C^{3+} into C^{4+} was 2×10^{18} m^{-2} s^{-1}. Hence the C^{3+} production flux is higher by two orders of magnitude than C^{3+} loss flux, suggesting that the C^{3+} population around the X-point is diminished due to effects not included in the present model yet such as transport related loss channels. The transport loss mechanism will be investigated with an improved impurity transport code such as IMPMC [9].

From the above evaluation, it is concluded that the dominant radiator, C^{3+}, is produced by ionization of C^{2+} and recombination of C^{4+} at similar rates around the X-point in the detached plasma. Because the ionization flux of C^{3+} is much smaller than the recombination flux of C^{4+} around the X-point, the predominant source of C^{4+}, which recombines into C^{3+}, is presumably the main plasma. Since the flux of C^{4+} is determined by the transport in the main plasma, it is difficult to control the C^{4+} flux. In contrast, significant ionization of C^{2+} into C^{3+} and no recombination of C^{3+} into C^{2+} indicate that the source of C^{2+}, which ionized into C^{3+}, exists in the divertor region, which can be controlled more easily for instance by seeding CD_4. Because the source rate of C^{3+} from the main plasma (the recombination of C^{4+}) and the divertor (the ionization of C^{2+}) was found to be similar as described above, the radiation loss control by impurity seeding from the divertor may be possible although the controllability may not be high.

Acknowledgement

This work was partly supported by JPSP, Grant-in-Aid for Scientific Research for Priority Areas (19055005).

References

[1] H. Kubo, T. Sugie, et al., Plasma Phys. Control. Fus. 37 (1995) 1133.
[2] M.E. Fenstermacher, S.L. Allen, et al., Phys. Plasmas 4 (1997) 1761.
[3] C.F. Maggi, J.D. Elder, et al., J. Nucl. Mater. 241–243 (1997) 414.
[4] T. Nakano, H. Kubo, et al., Nucl. Fus. 47 (2007) 1458.
[5] H. Kubo, T. Sugie, et al., Rev. Sci. Instrum. 59 (1988) 1515.
[6] T. Sugie, H. Kubo, et al., JAERI-M 93-057 Jpn. Atom. Energy Res. Inst. (1993) 347.
[7] U. Safronova, T. Kato, M. Ohira, J. Quant. Spectrosc. Radiat. Trans. 58 (1996) 193.
[8] M. Goto, K. Sawada, et al., Phys. Plasmas 9 (2002) 4316.
[9] K. Shimizu, T. Takizuka, et al., J. Nucl. Mater. 390–391 (2009) 307.